university of groningen

University Medical Center Groningen

University of Groningen

Spin Accumulation in Ferromagnetic/Normal and Ferromagnetic/Superconducting Systems

Zaffalon, Michele

IMPORTANT NOTE: You are advised to consult the publisher's version (publisher's PDF) if you wish to cite from it. Please check the document version below.

Document Version
Publisher's PDF, also known as Version of record

Publication date:
2006

Link to publication in University of Groningen/UMCG research database

Citation for published version (APA):
Zaffalon, M. (2006). *Spin Accumulation in Ferromagnetic/Normal and Ferromagnetic/Superconducting Systems*. s.n.

Copyright
Other than for strictly personal use, it is not permitted to download or to forward/distribute the text or part of it without the consent of the author(s) and/or copyright holder(s), unless the work is under an open content license (like Creative Commons).

The publication may also be distributed here under the terms of Article 25fa of the Dutch Copyright Act, indicated by the "Taverne" license. More information can be found on the University of Groningen website: https://www.rug.nl/library/open-access/self-archiving-pure/taverne-amendment.

Take-down policy
If you believe that this document breaches copyright please contact us providing details, and we will remove access to the work immediately and investigate your claim.

Downloaded from the University of Groningen/UMCG research database (Pure): http://www.rug.nl/research/portal. For technical reasons the number of authors shown on this cover page is limited to 10 maximum.

Download date: 06-05-2023

Chapter 3

Spin injection in 0D systems: experimental results

We present experimental results of spin accumulation in a small island of aluminium, with all lateral dimensions shorter than $\lambda_{\rm sf}$. Four cobalt contacts are connected to the island through tunnel barriers. We will show that for the system we fabricated, the spin accumulation is uniform throughout the island and can be described in terms of the relative orientation of the ferromagnetic contacts. From precession measurements at room temperature, we can extract the spin relaxation time $\tau_{\rm sf} = 60$ ps and the spin polarisation of the tunnel barriers $P = 8$ %. We begin by explaining the idea of the experiment and we then carry on to describe the sample preparation and to present spin valve measurements, at room temperature and at 4.2 K. Precession measurements are an invaluable tool to extract informations, not only about $\tau_{\rm sf}$ and P, but also about the magnetic orientation of the contacts.

3.1 Idea of the experiment

Previous measurements of Jedema *et al.* (2003) showed that the spin relaxation length in diffusive aluminium at room temperature is about $\lambda_{\rm sf} = 500$ nm. We fabricated and studied the spin accumulation inside an island with all dimensions shorter than $\lambda_{\rm sf}$. The spatial dependence of the spin accumulation can be neglected and the dynamics of uniform spin imbalance becomes independent on the electron transport properties, such as the diffusion constant. We call such a system zero-dimensional. We find that in a see of unpolarised electrons, some 1000 spin polarised electrons (one in 10^6), distributed uniformly within the island, move coherently for a time of the order of 100 ps.

In terms of characteristic times, the alternative equivalent way of looking at it is the following: in a zero dimensional system, the electron diffuses through the entire island before relaxing, $\tau_D < \tau_{\rm sf}$. The time scale τ_{esc} is the average time to escape from the island into the contacts. One may ask how it compares to τ_D and $\tau_{\rm sf}$. It turns out that the tunnel barriers we could fabricate are opaque

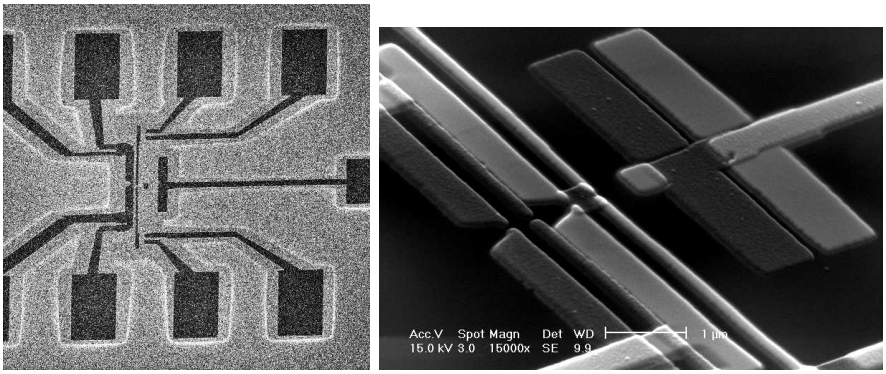

Figure 3.1: Left: the Ge mask ready for metal deposition. The Ge is etched-through in correspondence to the darker regions, leaving the substrate uncovered. The top polymer layer is completely removed. The bottom polymer layer is partially present

enough that electrons will leave the island well after they have lost their spin memory, $\tau_{esc} \gg \tau_{\rm sf} > \tau_D$. In this limit, spin accumulation can be described in an elementary way as the result of two competing processes: the injection of spins and their dynamics and relaxation.

3.2 Device preparation

The devices are prepared by shadow evaporation technique: this technique was first reported by Dolan (1977) to fabricate Al-based single electron transistors. For our devices, the high reactivity of Al and Co calls for a method that allows the evaporation of the bottom Al layer, the controlled oxidation to form the tunnel barriers, and the deposition of the second Co layer, all that without breaking the vacuum.

The trick is done by suspending a mask, see Fig. 3.1(left) some 1.6 μm above the substrate; the metals are evaporated and deposited through the mask onto the substrate under different angles, therefore creating different projections of the mask. After removal of the mask, the device looks similar to that of Fig. 3.1(right). The two replicas of the mask are visible: the light material is Co. The island and the four cobalt contacts are highlighted by the white circle.

We proceed as follows, see Fig. 3.2:

- the mask is realised by electron beam lithography: an electron sensitive polymer (PMMA-MMA AllResist AR-P 617.12, baked 1 hour in oven at 190 °C) is spun onto an insulating SiO_2 substrate (usually 500 nm of wet thermally grown on a 2 inches Si wafer), producing a 1.6 μm thick layer;
- 40 nm of Ge are evaporated on top of the uniformly flat layer of resist. The Ge layer will form the actual mask as it has the required mechanical strength to form the largely suspended mask;
- a second polymer layer (PMMA AllResist 950K AR-P 671.04) is then spun onto the Ge. It has lower electron sensitivity than the bottom layer,

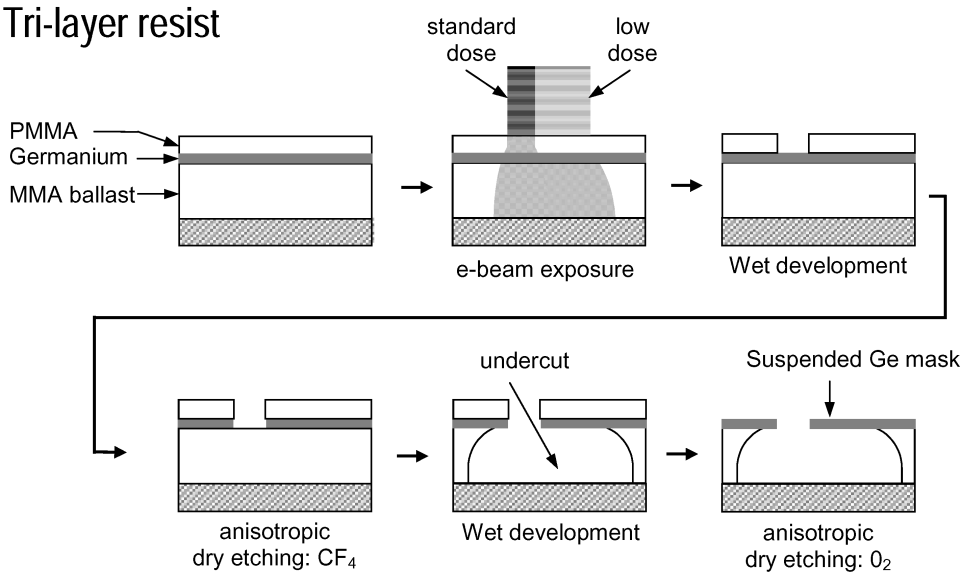

Figure 3.2: Schematic representation of the Ge mask preparation for shadow deposition: note the use of two different doses for the exposure of the resist in order to create an undercut. Taken from Jedema (2002).

allowing the possibility of exposing the bottom layer without affecting the top one. In this way, by carefully dosing the electron beam intensity, we can create cavities (undercuts) beneath the Ge: this is necessary to deposit the metals under large angles;

- after patterning the tri-layer by electron beam (JEOL 840, beam blanker and software from Raith), the top polymer is developed in a solution of MIBK and IPA 1:3 for 45 sec. The Ge is processed in a reactive ion etcher (first, a short oxygen descum (15 sec at 40 W) is followed by the etching with CF_4 gas, while the process is monitored by laser interferometry). The bottom layer is developed in MIBK:IPA 1:5 for 50 sec. Oxygen descum of the substrate follows, 3 min at 40 W. Descum steps are done to remove organic resist remains. The final mask is shown in the SEM micrograph, Fig. 3.1. Undercuts are also visible in Fig. 3.1(left), delimited by the whitish contour around the etched through (dark) regions;

- the deposition of the metals take place in a electron beam evaporator (Airco Temescal, with base pressure of 10^{-7} mbar): first, we deposit the island, 30 nm of Al at a rate between 0.1 and 0.3 nm/sec, with the chamber pressure raising to $2 \cdot 10^{-6}$ mbar during deposition. The tunnel barriers are formed by oxidation in a pressure of 10^{-2} mbar for a few minutes in native oxygen. Then the Co contacts, 40 nm thick, are deposited under a different angle, such as to contact the island. Standard lift-off in hot acetone, rinsing of the devices and bonding follow.

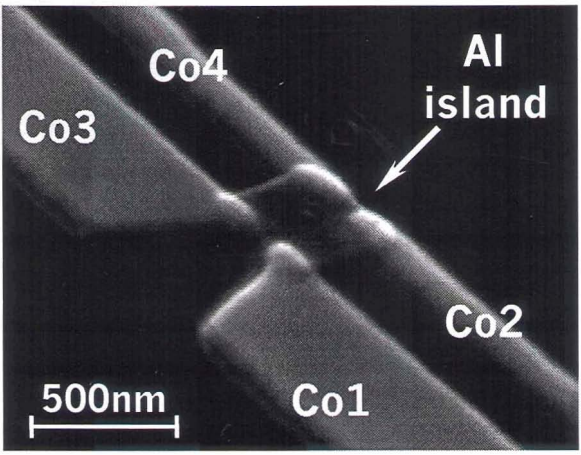

Figure 3.3: SEM micrograph of the device. The shadow replicas have been removed for clarity.

As mentioned above, the use of Al for the island is imposed by two constraints: a physical one, the choice of a material with low spin-orbit coupling (see Sect. 2.3), and a technological one, the ease of deposition, fabrication of tunnel barriers with high breakdown voltage and the formation of a self protecting layer when Al is exposed to air. Especially for this second reasons, Al_2O_3 has been extensively studied and used commercially for the preparation of magnetic tunnel junctions.

We aimed at the fabrication of tunnel barriers with resistances of the order of 1–10 kΩ, corresponding to resistances of $\approx 50\ \Omega\mu m^2$ and a transmission probability per conducting channel of $\approx 10^{-4}$. Measurements of the barrier in the superconducting state (see Chapter 6) will show that, for the more transparent interfaces, the oxide layer is not uniform. In fact it presents regions of clean contact between the two metals of the junction (pinholes). This does not impede the observation of a finite degree of spin polarisation.

3.2.1 Device characterisation

Each junction is first characterised by recording its I–V characteristic in a three terminal configuration: for instance, with reference to Fig. 3.3, we measure TB1 by sending current from Co1 to Co2 and measuring voltage between Co1 and Co3. All devices fabricated have either tunnel barriers with resistances in the range $2 - 30$ kΩ or clean contacts. The resistance of the Co electrodes is 20 and 90 Ω far the widest and the narrowest respectively. The device tunnel barriers are rather sensitive to electrostatic discharge and about 30% of the devices made (approx 50) were unusable due to the breakdown of one or more barriers. Even with careful handling (learnt by experience), the lifetime of a device was sometimes only a few days of measurements. Only in one case, a device survived 3 weeks of constant measuring.

The I-V characteristic of a single tunnel barriers measured at 4.2 K is shown

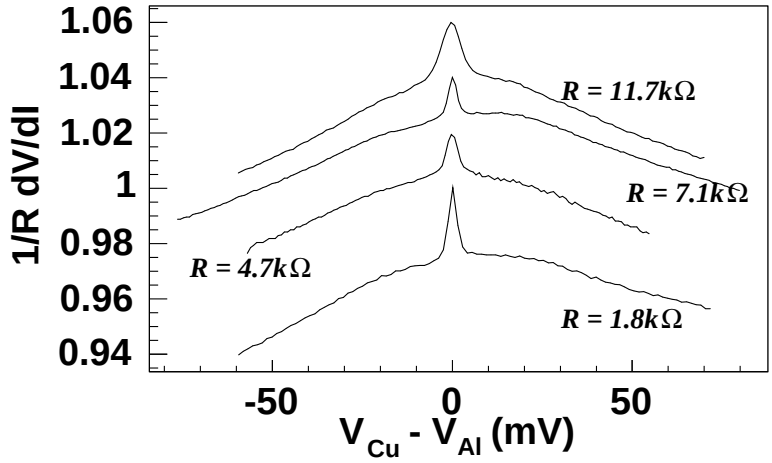

Figure 3.4: Normalised differential resistance of 1.8, 4.7, 7.1 and 11.7 kΩ tunnel barriers at 4.2 K. Traces are offset for clarity.

in Fig. 3.4. We note two features: all curves are asymmetric in the bias voltage, as the two metals (Co and Al) on each side of the junction have different work functions; the resistance decreases by less than 10 % in the range of interest (100-300 mV). Similar asymmetries have been observed in magnetic tunnel junctions with a thick (bulk-like) dusting layer made of non-magnetic metal (LeClair, 2002). The second feature is the pronounced peak at zero bias, which we have observed in all tunnel barriers with a ferromagnetic electrode measured at 4.2 K. We have not investigated its origin.

3.3 Spin transport in the island

The system is schematically represented in Fig. 3.5(a): four ferromagnetic electrodes Co1 through Co4, contact the island at its four corners, through tunnel barriers. We now study the four terminal resistance as a function of the magnetisation direction of the four contacts, in two different but not completely equivalent ways: in the first one, assuming collinear magnetisation, we use the resistor model. In the second one, with non-collinear magnetisation, in the spirit of the "finite element" approach (Brataas *et al.*, 2000), we neglect any spatial dependence of the spin dependent chemical potential and the spin current that originates from the gradient of $\boldsymbol{\mu}$. This weak spin current is automatically included in the first approach.

The resistor model approach to the island

In the resistor model picture, the island may be represented as the resistor network, Fig. 3.5(b), the resistors marked by r are the spin independent resistances of the normal metal, $\approx 2(\sigma_N/2)^{-1}L/A$; the majority/minority electron resistance of the tunnel barrier is $R^{+,-} = R_I(1 \pm P)/2$, with R_I the interface

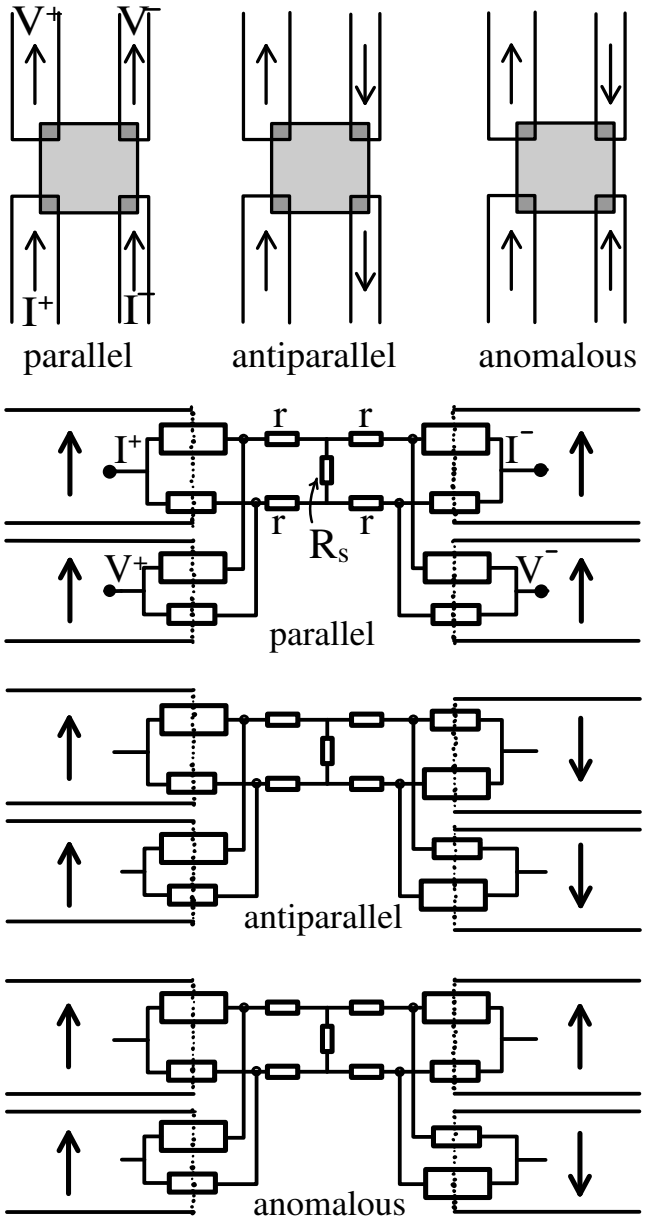

Figure 3.5: Top: Schematic representation of the island with the three possible magnetic orientations: parallel, antiparallel and anomalous. I^+ and I^- are current electrodes; V^+ and V^- are voltage probes. The position of I^+, I^-, V^+ and V^- represents one of the possible measuring configurations. Bottom: The equivalent resistor model in the three magnetic configurations. In all pictures, arrows represent the direction of the electrodes magnetisation.

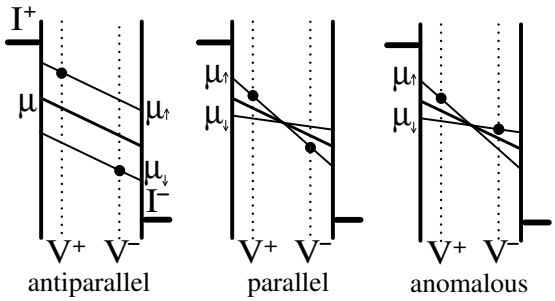

Figure 3.6: The chemical potentials $\mu_\uparrow = \mu + |\boldsymbol{\mu}|$ and $\mu_\downarrow = \mu - |\boldsymbol{\mu}|$ inside the island for the *side* configuration in the *antiparallel*, *parallel* and *anomalous* cases, assuming collinear magnetisation. We remind that only for antiparallel injectors, is $|\boldsymbol{\mu}|$ uniform (see main text). The lines represent the spin up and down chemical potentials $\mu_{\uparrow,\downarrow}$ and the thick line the average μ. The black dots indicate the potential measured by the V^+ and V^- probes for $P = 1$.

resistance, assumed equal for all contacts. The interface resistors for the individual channels have dimensions proportional to their conductance. $R_{\rm sf}$ is the spin resistance as found in Sect. 2.7.

In the collinear case, there are three possible independent magnetic configurations: a *parallel*, an *antiparallel* and an *anomalous*, Fig. 3.5. A second anomalous configuration is with the widest electrodes having antiparallel orientation and the narrowest parallel, but it is equivalent, by the reciprocity theorem, to the drawn one. Below are shown the corresponding resistor model configurations, see Fig. 3.5.

Let us start with the antiparallel configuration, with the resistances arranged as in the figure: both spin channels have the same resistance, and $I_\uparrow = I_\downarrow$. The four terminal resistance is ($R_{\rm sf},\ R_{Ohm} \ll R_I$)

$$R_{AP} = R_{Ohm} + P^2(R_{\rm sf} + R_{Ohm}) \tag{3.1}$$

where $R_{Ohm} = r$. In the parallel case, a spin current is the result of the two spin channels having different resistance, which produce a different voltage drop for the two channels. Their difference in resistance is proportional to the island Ohmic resistance, $R_{Ohm}(I_\uparrow - I_\downarrow) \approx PR_{Ohm}I$ (in the detected signal, an additional P comes from the detection efficiency):

$$R_P = R_{Ohm} + P^2 R_{Ohm}. \tag{3.2}$$

The spin induced signal is a fraction of the Ohmic resistance. If $P = 1$, the total resistance doubles, because only one spin channel is used, halving the island's conductance. From the definition of zero-dimensional system, $\tau_{\rm sf} \gg \tau_D$, we conclude that the spin induced signal in the antiparallel configuration is larger than in the parallel one, $P^2 R_{\rm sf} > P^2 R_{Ohm}$.

In the anomalous configuration, the signal is the Ohmic background and the lowest of the three configurations

$$R_{anom} = R_{Ohm}. \tag{3.3}$$

These results are strictly valid only in the limit of collinear electrodes. We analyse the situation for a strictly 0D system with non-collinear electrodes.

The finite element approach to the island

The idea behind the second approach is that we can solve the transport equations in the bulk materials, (for ferromagnets, $\mu_{\uparrow,\downarrow}(x)$, for non-magnetic metals, $\mu(x), \boldsymbol{\mu}$), with the boundary conditions imposed by the charge and spin currents through the interfaces. In turn, charge and spin currents are determined by the chemical potentials on each side of the interface. For tunnel barriers, the ratio spin current to charge current is P, eq. (2.27). We proceed in the following way: first we note that the detected signal $\mu_F = \mu_N + P\mathbf{m}\cdot\boldsymbol{\mu}$ has an Ohmic contribution (the spin independent part) and a spin dependent contribution. We calculate these two contribution separately.

The spin independent chemical potential is position dependent and obeys

$$\nabla^2\mu(x) = 0 \tag{3.4}$$

with the boundary conditions given only by the charge current I entering the island. Were not the voltage contacts FM3 at x_3 and FM4 at x_4 spin sensitive

$$\frac{\mu_3^F - \mu_4^F}{eI} = \frac{\mu(x_3) - \mu(x_4)}{eI} = R_{Ohm} \tag{3.5}$$

this is the island four-terminal resistance, independent on the magnetic configuration of FM1 and FM2 (Hall effects are totally ignored, here, as for *metallic* system, the Hall coefficient is negligeable, see 3.3.1). In the stationary state, spin conservation requires

$$\frac{1}{\nu_D\hat{V}}\sum_j \mathbf{i}_j = \frac{\boldsymbol{\mu}_a}{\tau_{\rm sf}} + \frac{g\mu_B}{\hbar}\mathbf{B}\times\boldsymbol{\mu}_a \tag{3.6}$$

where $\mathbf{i}_j$ is the spin current through contact j: $\mathbf{I} = (P_1\mathbf{m}_1 - P_2\mathbf{m}_2)\mu_B I/e \equiv \mathbf{s}\mu_B I/e$, the minus sign because the charge current leaves the island through FM2. $|\mathbf{m}_i| = 1$ is a unit vector. $\mu_3^F - \mu_4^F = \mu(x_3) - \mu(x_4) + (P_3\mathbf{m}_3 - P_4\mathbf{m}_4)\cdot\boldsymbol{\mu}_a$. The total signal for $|\mathbf{B}| = 0$ is

$$R = \frac{\mu_3^F - \mu_4^F}{eI} = R_{Ohm} + R_s \quad \text{with} \quad R_s = \frac{\tau_{\rm sf}}{\nu_D e^2\hat{V}}\mathbf{s}\cdot\mathbf{d} \tag{3.7}$$

the detector defined as $\mathbf{d} \equiv P_3\mathbf{m}_3 - P_4\mathbf{m}_4$. $\nu_D = 2.4\cdot 10^{28}$ eV^{-1}m^{-3} is the aluminium density of states at the Fermi energy. In a true antiparallel configuration (and all P_i equal), $R_s = 4P^2\tau_{\rm sf}/\nu_D e^2\hat{V}$, a result obtained also with the first method. If $\mathbf{s} = \mathbf{0}$ or $\mathbf{d} = \mathbf{0}$, the detected signal is the background Ohmic resistance. Any other configuration can be understood in terms of the relative orientation between $\mathbf{s}$ and $\mathbf{d}$.

One may wonder what happens if $\tau_{\rm sf}$ becomes very long: eq. (3.7) predicts that the spin signal increases without bounds. This comes from the assumption, while writing $\mathbf{j}_s$ as function of j, we ignored the spin accumulation both in the non-magnetic metal and in the ferromagnetic contacts, eq. (2.19) (for the non-collinear case, see Chapt. 4). Spin accumulation partially blocks one spin channel so as to limit the injected spin current.

This can be shown using the resistor model. The spin imbalance reads

$$\mu_z = \frac{PI/2}{\frac{1}{R_{\rm sf}} + \frac{4}{R_I}\left(1 + \frac{r}{R_{\rm sf}}\right)} \tag{3.8}$$

saying that the limiting mechanism is a fictious relaxation through the resistors R_I, or in other words, the leaking of spins through the contacts. The factor 4 at denominator comes about because four junctions are connected to the island. We remind that in our island, the relaxation happens exclusively inside the island, as $R_I \gg R_{\rm sf}$.

It is now tempting to define τ_{esc} such that

$$R_I \equiv \frac{4\tau_{esc}}{\nu_D e^2 \hat{V}} \tag{3.9}$$

in the same way $R_{\rm sf}$ is related to $\tau_{\rm sf}$.

We show in Fig. 3.6 the chemical potentials inside the island in the three different configurations. We assume as in the resistor model, that all electrodes are collinear and all interfaces' polarisations are equal. The voltage is detected at the probes FM3 and FM4 and the black dots are the voltages that would be detected if $P = 1$. Differently from the resistor model, we have allowed for some potential drop between I^+ and V^+, and between I^- and V^-.

We are ready to prove again eq. (3.2), here with a different argument. As stated before, in the parallel configuration, there is no net spin accumulation. However, a spin *current* $|\mathbf{I}| = PI\mu_B/e$ is injected at I^+ and extracted at I^-, giving rise to a space dependent magnetisation, $|\mathbf{I}| = -(\sigma_N \mu_B/e)\cdot\nabla(\mu_\uparrow - \mu_\downarrow)/2$, σ_N being the Ohmic conductance of the island in much the same way a charge current generates a space dependent chemical potential, $I = -(\sigma_N/e)\nabla\mu$. Recalling that the device is in the parallel configuration, the detected spin related contribution is P times the difference of the spin up chemical potential at the V^+ and V^- positions, $R_s = P^2 R_{Ohm}$.

In the anomalous configuration, the V^+ probe measures $\mu_\uparrow$ and V^- detects $\mu_\downarrow$. Owing to the symmetric position of V^+ and V^- with respect to I^+ and I^-, both probes measure the same amount of magnetisation and giving no spin dependent contribution, $R_s = 0$. In the anomalous configuration, one therefore expects to have the lowest signal, equal to the island's Ohmic resistance.

3.3.1 Spin accumulation and spurious effects

Spurious effects can hide or mimic spin accumulation. For instance, the fringe field of the ferromagnetic electrodes may produce not only precession of the local spin accumulation, but also local Hall effects. Reversing the magnetisation reverses also the sign of the Hall voltage, in the same way the spin accumulation does. Whereas in semiconducting systems, care has to be taken to avoid that, owing to the large Hall coefficients of low electron density conductors (Monzon *et al.*, 1997), in metallic systems, this is of less concern. For an estimate of the order of magnitude, taking the Hall resistance $R_H = -3.5 \cdot 10^{-11}$ Ωm/T for Al in the low field limit (Ashcroft and Mermin, 1976), the Hall contribution would be $R_H B/d \approx 0.1$ mΩ, using the thickness of our devices $d = 30$ nm and a typical fringe field of $B = 100$ mT. In general, the spin induced signals are much larger than this.

In the clean contact regime, AMR (Sect. 2.1.2) can contribute to the detected signal at a voltage contact in a subtle way: although no *net* current is drawn by the ideal voltage contact, current does flow in the ferromagnet (Fert and Lee, 1996) causing additional voltage drop. The point is that the resistance of the ferromagnet is sensitive to the angle θ between the local magnetisation and the flowing current. This may be a concern if the direction of the ferromagnet is not well defined, as for instance, during magnetisation reversal, and the spurious contribution from AMR (1% of the ferromagnet resistance or so) can hide the spin induced signal. This is avoided in four terminal measurements on devices with tunnel barriers as there is no current flowing across the voltage contacts.

3.4 The measuring setup

Four terminal measurements are done in standard lock-in configuration: an ac voltage modulation from a SR830 lock-in is fed to a homemade voltage-to-current converter and the current ($10 - 100$ μA rms) sent to the device. The voltage signal V is amplified usually 100 times by a homemade voltage amplifier and measured with the lock-in.

Voltages applied to the junctions should not exceed the breakdown voltage, 300 mV, limiting the current to 100 μA.

Capacitive coupling between leads is particularly severe in the "diagonal" configuration, because the measured resistance is smaller (no Ohmic background). To reduce their influence, all measurements are performed at 4 Hz. Capacitive coupling introduces, at relative high measuring frequencies, only a systematic error that drops out if one is only interested in resistance differences, $R_{AP} - R_P$, $R_{anom} - R_P$....

Most of the measurements in this chapter are taken at room temperature. The measurements at 4.2 K employed the same electrical setup, and a dipstick to hold the sample inside a 4.2 K cryostat. A magnetic field sufficient to flip the electrodes' magnetisation is provided by a 300 mT non-superconducting coil fit inside the cryostat. Measurements with the Al in the superconducting state are described in Chap. 6.

3.5 The spin valve measurements

We present here experimental results of spin injection and accumulation in the following order:

- spin valve measurements in the side, diagonal and opposite measuring configurations, in devices with tunnel barriers, see 3.5.1 and 3.5.2

- precession measurements in order to extract the polarisation P, $\tau_{\rm sf}$ and the orientation of the electrodes' magnetisation, Sect. 3.6;

- the reciprocity theorem for the spin accumulation, showing that one has to interchange voltage with current contacts and reverse all magnetic fields, included the electrodes' magnetisations, Sect. 3.7;

- measurements at 4.2 K on devices with tunnel barriers and comparison with devices with clean contacts, Sect. 3.8. The comparison with the clean

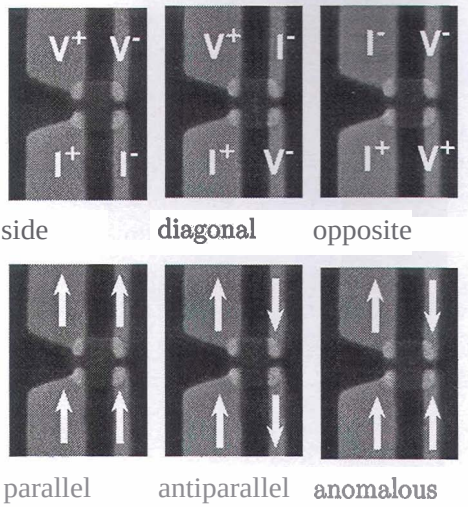

Figure 3.7: above: The three possible independent electrical configurations: Current is sent from I^+ to I–, the detected voltage is $V = V^+ - V^-$. below: The three magnetic configurations.

contacts devices, in particular, shows how the spin signal is reduced by the diminished efficiency of the injectors/detectors.

We have measured 16 devices, three at 4.2 K only, four (two with clean contacts, 1 H-shaped with tunnel barriers) both at 4.2 K and at room temperature, and nine at room temperature only. Chronologically we carried out first the low temperature measurements on devices with highly resistive tunnel barriers (5–30 kΩ); precession measurements could not be performed because of technical difficulties with the rotating stage of the dipstick. On these devices, the tunnel barriers showed a very short life (one day) and in most cases, they did not survive thermal cycling to room temperature. In a second time, we started fabricating devices with transparent tunnel barriers, the lowest 700 R, and measured them at room temperature only. We show a set of representative measurements at room temperature on one device with two tunnel barriers of 850 Ω and two of 1.6 kΩ. At the end of thii Chapter, we compare them with measurements on other devices both at room temperature and at 4.2 K.

Two-terminal measurement, GMR like, are totally dominated by the tunnel barriers resistances, and independent *on* the contact's magnetisation direction. In a four-terminal measurement, see Fig. 33, there are three independent measuring configurations. The current I is sent between I^+ and I^- and the detected voltage is $V = V^+ - V^-$. The plotted signal is the ratio $R = V/I$. In the *side* configuration, the background is the island's Ohmic resistance. In the *diagonal* configuration, little Ohmic contribution is expected, owing to the symmetric position of the voltage contacts with respect to the current path. The spin dependent contribution in the two cases is however equal if the island is zero-dimensional. On the other hand, the *opposite* configuration should show small spin signal as the widest electrodes switch at the same time ($s \approx 0$) and so do the narrow ones ($d \approx 0$).

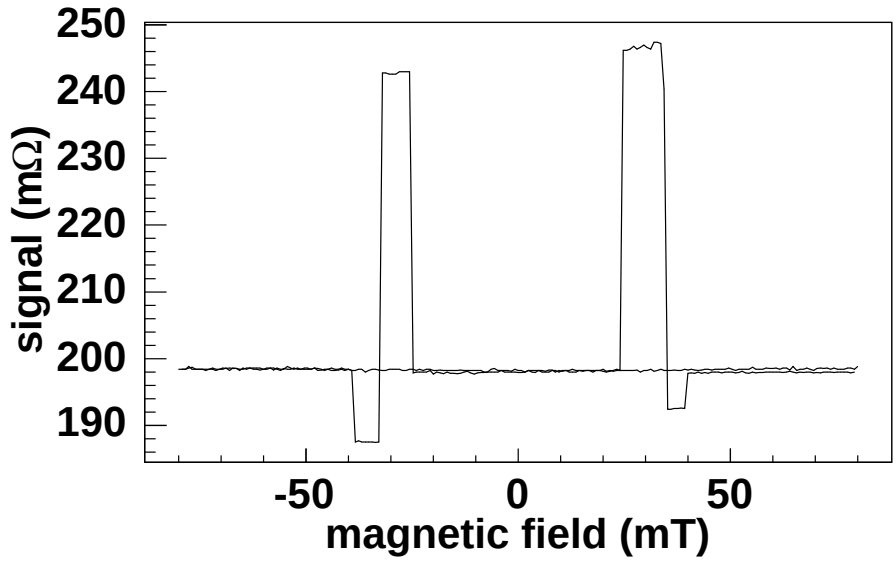

Figure 3.8: Spin valve in the side measuring configuration. The spin signal is 48 mΩ. The background signal at 198 mΩ is the Ohmic resistance of the island.

3.5.1 The side configuration

A *spin valve* device is so called because the change of the magnetic orientation of the FM contacts causes a change in the (four terminal) resistance. Fig. 3.8 shows a measurement in such a device.

We record the resistance while applying a magnetic field in plane, in the $\hat{\mathbf{y}}$ direction. Starting with a negative magnetic field of –80 mT, with all the contacts having magnetisation parallel to each other, we sweep the field to positive values. When the switching field of the widest Co electrodes is reached, at +25 mT, Co1's and Co3's magnetisations reverse, the magnetic configuration is *antiparallel*, and the detected signal increases above the background level by 45 mΩ. Increasing the field further, at −32 mT, one of the smaller electrodes reverses, and the signal dips 10 mΩ below the background level. At −38 mT, the second smallest electrode also flips and the signal reaches the background value. The reverse trace shows very similar behaviour, the notable difference being a larger peak, about 48 mΩ, and a smaller dip, 6 mΩ. Repeated sweeps give similar results.

Under the assumption that all P_i are equal, the spin signal $R_s \propto P^2\tau_{\mathrm{sf}}$. With only spin valve measurements, we cannot extract separately $|P|$ and τ_{sf}. Precession measurements do allow that but they do not clarify the sign of P.

We want to point out here, that the terms parallel and antiparallel are only useful shorthand notations for the magnetic configuration. The contacts' magnetisation are non-collinear (this will turn out from the precession measurements) and the correct description is in terms of the vectors $\mathbf{s}$ and $\mathbf{d}$. Interestingly, eq. (3.7) tells that the spin signal is invariant if $\mathbf{s} \to -\mathbf{s}$ and $\mathbf{d} \to -\mathbf{d}$, which we expect when the contacts' magnetisation flips. This is contradicted by the experimental data that show the two peaks in the AP configuration (and dips in the anomalous) having different heights. In fact, we believe this

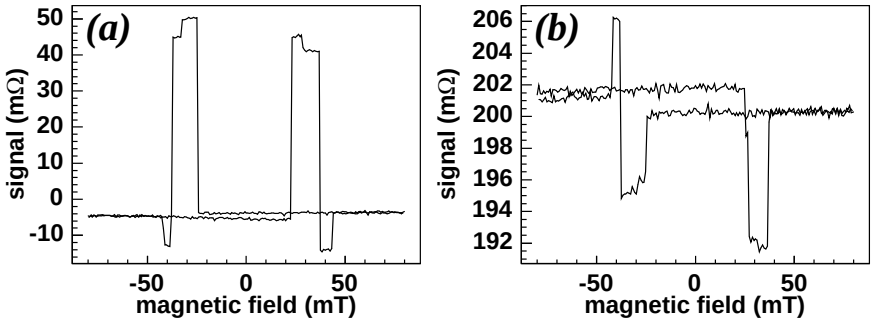

Figure 3.9: Spin valve in the diagonal and opposite measuring configurations. In the diagonal configuration, the spin signal is just larger than 50 mΩ, whereas in the opposite configuration about 10 mΩ.

discrepancy can be fully accounted for by assuming non-collinear electrodes.

The spin valve measurements alone are somewhat of limited utility. For instance, we cannot tell whether the contacts are collinear. If they were, the dip in the anomalous configuration can only be originated by the spin current, eq. (3.2). The ratio dip to peak heights, eq. (3.1) and eq. (3.3) is $\approx P^2$. Precession measurements will show that $P = 7\%$ and that the spin current may only account for a voltage drop of $P^2 R_{Ohm} \approx (0.07)^2 \times 200\ \mathrm{m\Omega} = 1\ \mathrm{m\Omega}$.

3.5.2 The diagonal and opposite configurations

Alternatively, we perform a spin valve measurement in the *diagonal* measuring configuration. The result is shown in fig. 3.9(a). A similar behaviour as for the side configuration is visible with a spin signal of 55 mΩ. This allows us to conclude that the spin accumulation is uniform within the island, as the spin induced signal is independent on the position we measure it. Note that around zero magnetic field, with parallel configuration, the traces are offset by some 2 mΩ.

In the last independent measuring configuration, see Fig. 3.9(b), a small spin signal of 10 mΩ is detected because the large electrodes flip at the same time, and $\mathbf{s} \approx \mathbf{0}$.

3.5.3 The memory effect

The ferromagnetic contacts are hysteretic: in the spin valve measurements, we needed some 30 mT at room temperature to reverse the contact's magnetisation. Based on this fact, we performed measurements to show what we call the *memory effect*. We started with the antiparallel configuration at +30 mT (the largest electrodes magnetisation pointing in the $+\hat{\mathbf{y}}$ direction) and we sweep toward negative magnetic fields. The electrode retains the antiparallel configuration until we reach –25 mT, at which point the largest electrodes switch parallel to the small ones. In the reverse sweep, the largest electrodes flip again at +20 mT, returning to the initial configuration.

The other trace is the memory effect in the anomalous configuration. We start at +33 mT. Let us suppose Co1, Co2 and Co3 are parallel to the $\mathbf{y}$ direction

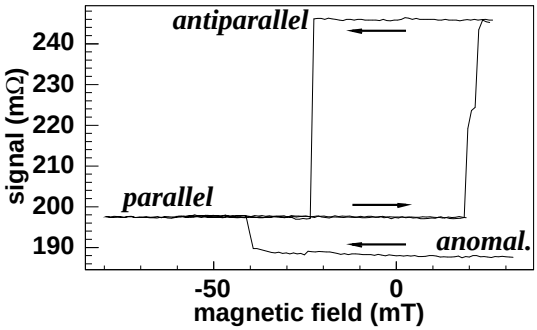

Figure 3.10: The memory effect in the side geometry in the antiparallel (upper trace starting at 246 mΩ) and in the anomalous (lower trace from 186 mΩ) configuration. The arrows show the direction of the magnetic field sweep.

and Co4 is opposite and we sweep the field toward negative values. At –25 mT, the largest electrodes Co1 and Co3 flip, now pointing in the $-\mathbf{y}$ direction. This is still an anomalous configuration, and the signal remains constant. At –40 mT, also Co3 reverses and the system is now in the parallel configuration with the signal at its background level.

3.6 The precession measurement, or Hanle measurement

Precession measurements, although more complicated than the spin-valve measurements, give a wealth of information, such as $\tau_{\rm sf}$ and the efficiency of the injectors/detectors, as well as information on the relative angles between the contacts' magnetisation. Besides, by using precession as a way of manipulating spins, our experiment can be defined a *polarise/analyse* experiment, where we prepare the system in a particular state, we let it evolve in time and we detect its final state.

We proceed in the following way: first, we set the magnetic configuration by applying the field in the $\hat{\mathbf{y}}$ direction, to parallel, antiparallel or anomalous. Then with the $\hat{\mathbf{y}}$ field switched off, we apply the magnetic field along $\hat{\mathbf{z}}$. A typical measurement for the side configuration is shown in Fig. 3.11, for the three magnetic cases, parallel, antiparallel and anomalous.

For both the antiparallel and the anomalous case, there is a noticeable dependence on the magnetic field, whereas for the parallel case, little modulation is seen. For fields up to 300 mT, the resistance trace is smooth, meaning the magnetic configuration is stable. For higher fields, however, the electrodes magnetisation tend to flip and the measured signals present sudden jumps. We cannot exclude that the magnetisation moves coherently even before 300 mT.

One could think of doing precession measurements with an in-plane magnetic field, perpendicular to the leads, in the $\hat{\mathbf{x}}$ direction. The left inset in Fig. 3.11 shows the result of such a measurement, when the field is swept from +40 mT

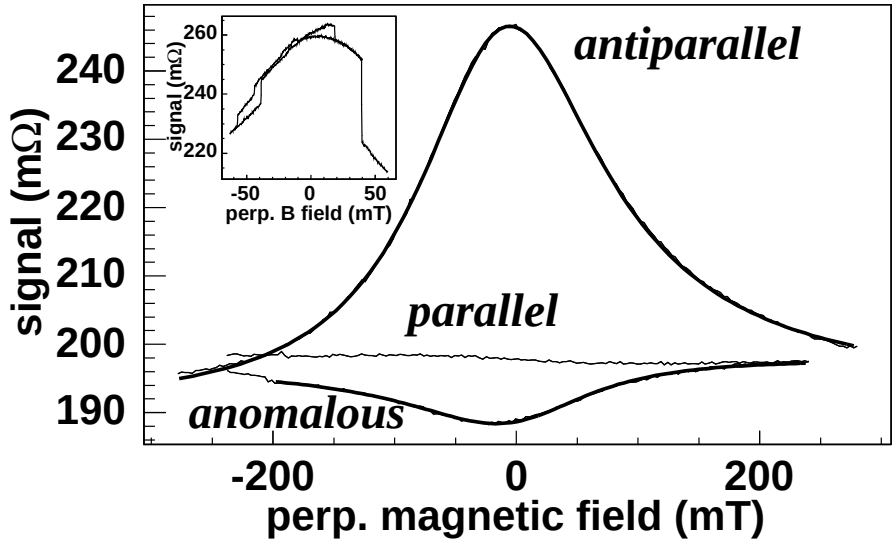

Figure 3.11: Precession in the side measuring configuration, in the antiparallel (top trace), parallel (middle) and anomalous (bottom) magnetic configurations. The fit with eq. (3.12) is superimposed to the antiparallel and anomalous traces and follows closely the experimental data. The left inset shows a precession measurement with an in-plane magnetic field, perpendicular to the leads, in the $\hat{\mathbf{x}}$ direction: at fields as low as |30| mT, the electrodes' domains begin to rotate and the signal becomes jerky, making it impossible to reliably extract τ_{sf}.

to –60 mT: at fields as low as |30| mT, the electrodes' domains begin to rotate and the signal deviates from a smooth curve.

Under the external magnetic field, the spins injected in the island precess and the detected spin signal reaches zero, when the average precession angle is $\pi/2$ to the detector.

The solution of eq. (3.6), written in terms of $\boldsymbol{\omega} = g\mu_b\mathbf{B}/\hbar$, is:

$$\boldsymbol{\mu} = \frac{\tau_{\rm sf} I}{\nu_D e^2 \hat{V}} \left[\mathbf{s}_{||} + \frac{\mathbf{s}_\perp - \tau_{\rm sf}\boldsymbol{\omega}\times\mathbf{s}_\perp}{1+|\boldsymbol{\omega}|^2\tau_{\rm sf}^2} \right] \tag{3.10}$$

where $||$ means parallel to $\boldsymbol{\omega}$. The spin induced signal reads

$$R_s = \frac{\tau_{\rm sf}}{\nu_D e^2 \hat{V}} \left[\mathbf{s}_{||}\cdot\mathbf{d}_{||} + \frac{\mathbf{s}_\perp\cdot\mathbf{d}_\perp - \boldsymbol{\omega}\tau_{\rm sf}\cdot(\mathbf{s}_\perp\times\mathbf{d}_\perp)}{1+|\boldsymbol{\omega}|^2\tau_{\rm sf}^2} \right] \tag{3.11}$$

Note that the expression is symmetric in $\mathbf{s}$ and $\mathbf{d}$, as one expects from the reciprocity theorem. Assuming now that $\boldsymbol{\omega}$ is in the $\hat{\mathbf{z}}$ direction, $\boldsymbol{\omega} = \omega\hat{\mathbf{z}}$, we can rewrite eq. 3.11 in a more suitable way for interpolation:

$$R_s = \frac{\tau_{\rm sf}|\mathbf{s}_\perp||\mathbf{d}_\perp|}{\nu_D e^2\hat{V}} \frac{\cos\phi - \omega\tau_{\rm sf}\sin\phi}{1+\omega^2\tau_{\rm sf}^2} + R_{back} \tag{3.12}$$

where

$$R_{back} = R_{Ohm} + \frac{\tau_{\rm sf}\mathbf{s}_{||}\cdot\mathbf{d}_{||}}{\nu_D e^2\hat{V}}. \tag{3.13}$$

ϕ is the angle between the projection on the substrate plane of the source and detector vectors.

At this point, using ferromagnetic contacts, one has to be concerned with the fringe field generated by the electrodes themselves, that thread the island. To account for these, we add an extra term $\boldsymbol{\omega}_{st}$ to the external magnetic field, $\boldsymbol{\omega} = g\mu_b\mathbf{B}/\hbar + \boldsymbol{\omega}_{st}$. $\boldsymbol{\omega}_{st} \to -\boldsymbol{\omega}_{st}$ upon reversal of all the electrodes' magnetisations. We remind that eq. (3.11) is still valid provided $||$ and $\perp$ are interpreted as parallel and perpendicular to the *total* magnetic field $\boldsymbol{\omega}$.

Let us assume for the moment that also $\boldsymbol{\omega}_{st}$ is along $\hat{\mathbf{z}}$. Now, we are ready to fit the data with five free parameters: the spin relaxation time $\tau_{\rm sf}$, the angle ϕ, the perpendicular component of the stray field $\omega_{st,\perp}$, the background resistance R_{back}, and the coefficient $A = |\mathbf{s}_\perp||\mathbf{d}_\perp|/(\nu_D e^2\hat{V})$, which contains P^2.

For the antiparallel case, the fit eq. 3.12 follows the experimental points very closely and gives $\tau_{\rm sf} = 62 \pm 2$ ps, $\phi = (-0.06 \pm 0.01)\pi$, $\omega_{st} = -14 \pm 4$ mT and $R_{back} = 192 \pm 1$ mΩ. Using the diffusion constant for the aluminium $D = 5{\cdot}10^{-3}$ m^2/s that was obtained from resistance measurements, the diffusion time is $\tau_D = L^2/D \approx 30$ ps, shorter than $\tau_{\rm sf}$. The spin diffusion length $\lambda_{\rm sf} = \sqrt{D\tau_{\rm sf}} \approx 550$ nm.

We now give a first estimate of the polarisation P: assuming that only the widest electrodes' magnetisations are rotated by ϕ, inset of Fig. 3.11, $\mathbf{s}_\perp = \mathbf{d}_\perp = 2P\cos(\phi/2)$, we find $P = 7\%$ (we used $\hat{V} = 400\times400\times30$ nm^3 for the island volume).

The modulation of the signal in the anomalous configuration clearly indicates that also in this case spin accumulation occurs. We fit also this trace with eq. (3.12) but now fixing $\tau_{\rm sf}$ to the value found in the side antiparallel case (the above one). We find $\phi = (0.11\pm0.04)\pi$, $\omega_{st} = 0\pm8$ mT and $R_{back} = 197\pm1$ mΩ.

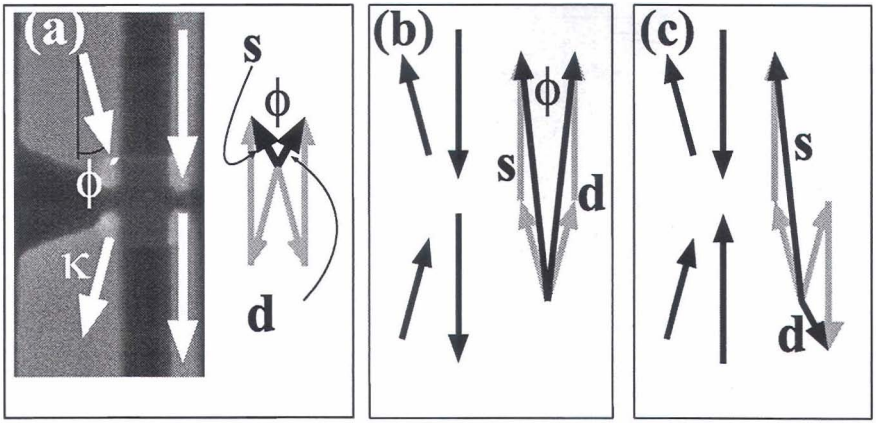

Figure 3.12: (a) Orientation of the electrodes' magnetisation in the parallel configuration. The quantity $(P_i\mathbf{m})_\perp$ for the widest electrodes is canted by an angle $4'$ with the direction of the narrow electrodes' magnetisation and is shorter by κ than the narrowest electrodes. On the right half of (a), the black arrows represent the injector $\mathbf{s}_\perp = (P_1\mathbf{m}_1 - P_2\mathbf{m}_2)_\perp$ and the detector $\mathbf{d}_\perp = (P_3\mathbf{m}_3 - P_4\mathbf{m}_4)_\perp$ for the side configuration, and ϕ being the angle between the two vectors $\mathbf{s}_\perp$ and $\mathbf{d}_\perp$. The same schematics for the antiparallel (b) and anomalous (c) configurations. Note that if all $|P\mathbf{m}|$ where equal, the angle between $\mathbf{s}_\perp$ and $\mathbf{d}_\perp$ is $\pi + \phi'$, ϕ' and $\frac{\pi}{2} + \phi'$ in the parallel, antiparallel and anomalous configuration respectively.

Note that for both the antiparallel and anomalous configurations, the fitting curves are showed on the graph.

Both ω_{st} and ϕ show variations between successive measurements, spanning from $|7|$ to $|15|$ mT and from $|0.04|\pi$ to $|0.07|\pi$ respectively, in the antiparallel side configuration. On the other hand, both the spin relaxation time and the polarisation show constant values throughout the time of the measurements.

We are now ready to find out the direction of the magnetisation: we have to rule out the possibility that all contacts have the same magnitude of $P\mathbf{m}_\perp$, because this would imply that in the anomalous configuration, the angle between s and d is $\frac{\pi}{2} + \phi \approx \frac{\pi}{2}$, as 4 is small, see Fig. 3.12. This in turn implies that in the anomalous configuration, the spin signal would cross R_{back} around $|\mathbf{B}| = 0$, which is not seen in the experimental data. We then assume that the largest electrodes have the component $(P\mathbf{m})_\perp$ smaller by a factor κ than for the smallest electrodes.

We now note that for the function

$$g(x) = \frac{\cos\phi - x\sin\phi}{1 + x^2} \tag{3.14}$$

$\max(g) - \min(g) = 1$ for every value of ϕ holds: the total modulation of the spin signal in the precession measurements is therefore proportional only to $|\mathbf{s}_\perp||\mathbf{d}_\perp|$, independent of the angle between injector and detector.

We show now that $\kappa = 0.7 \pm 0.1$, see Fig. 3.12, and that the angle $4'$ by which the largest electrodes are tilted inwards[1] is $\phi' = (0.08 \pm 0.01)\sim$ in the

[1]We remind that the angle ϕ is defined as the angle between the vectors $\mathbf{s}_\perp$ and $\mathbf{d}_\perp$.

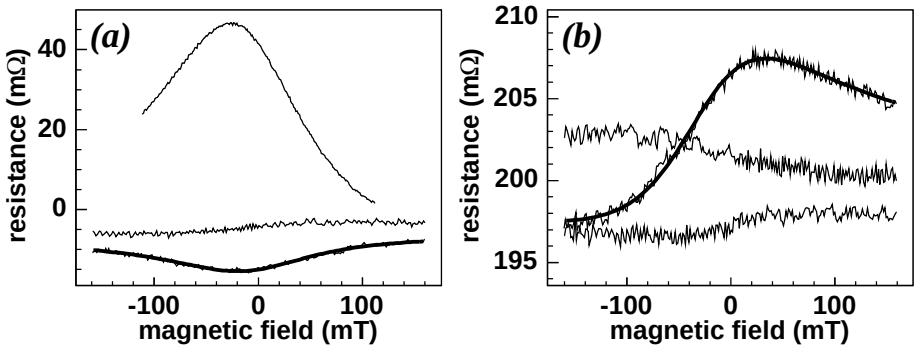

Figure 3.13: Precession measurements in the diagonal and opposite measuring configuration.

antiparallel case, $|\mathbf{s}_\perp||\mathbf{d}_\perp| \approx (1+\kappa)^2$ (as $\cos\phi' \approx 1$), and $\approx 1-\kappa^2$ in the anomalous. Their ratio $(1-\kappa^2)/(1+\kappa)^2 \approx 18\%$.

We show that this value is close to the experimental result. From the measurements in Fig. 3.11, we find the maximum modulation of the precession signal in the anomalous and antiparallel configuration, respectively 9 and 55 mΩ, and their ratio is 16%.

This is also compatible with the small modulation of the signal in the parallel configuration. In fact, the ratio between the amplitudes in the parallel and antiparallel signals $(3\ \text{m}\Omega/55\ \text{m}\Omega)^2 \approx 6\%$ is close to the expected ratio $(1-\kappa)^2/(1+\kappa)^2 = (0.30/1.70)^2 = 3\%$. The efficiency of the narrowest electrodes becomes $P = 8\%$, assuming that all contacts are lying on the plane $|\mathbf{m}_\perp| = 1$.

As we did for the spin valve measurements, we can perform precession measurements for the diagonal and opposite measuring configurations. Fig. 3.13 is the result for the antiparallel, parallel and anomalous configurations. As before, we fit with eq. (3.12), and we find the relevant parameters, $P = (8.0 \pm 0.5)\%$, $\tau_{\text{sf}} = 65 \pm 4$ ps consistent with those found in the side configuration, and $\omega_{st} = -13 \pm 4$ mT, $\phi = (0.10 \pm 0.02)\pi$ and $R_{back} = -8 \pm 1$ mΩ. For the anomalous configuration, we fit fixing the spin relaxation time to the value found in the (diagonal) antiparallel case as before, and we find $\phi = (0.08 \pm 0.05)\pi$, $\omega_{st} = -8 \pm 8$ mT and $R_{back} = -7 \pm 1$ mΩ.

In the opposite configuration, the most notable feature is a large modulation of the anomalous configuration and the fact that the signal is odd in the magnetic field, meaning that the $\mathbf{s}$ and $\mathbf{d}$ are perpendicular to each other. Again, we fit the data for the anomalous configuration by fixing $\tau_{\text{sf}} = 62$ ps, the values found in the side configuration, and we find $\phi = (-0.35 \pm 0.01)\pi$, $\omega_{st} = -23 \pm 7$ mT and $R_{back} = 200 \pm 1$ mΩ.

Also in this case, we compare the predicted signal in the opposite anomalous configuration $2 \times 2\kappa \sin\phi'$ with that of the *side antiparallel* configuration, $(1+\kappa)^2$: $(1+\kappa)^2/4\kappa\sin\phi' = 4.1$, to be compared with the experimental values $55\ \text{m}\Omega/10\ \text{m}\Omega = 5.5$.

With the value for the polarisation, we calculate the spin accumulation $|\boldsymbol{\mu}| = (\mu_\uparrow - \mu_\downarrow)/2 = R_s I/P \approx 50\ \mu$eV.

The value of the polarisation found, 8%, is 6 times smaller that the po-

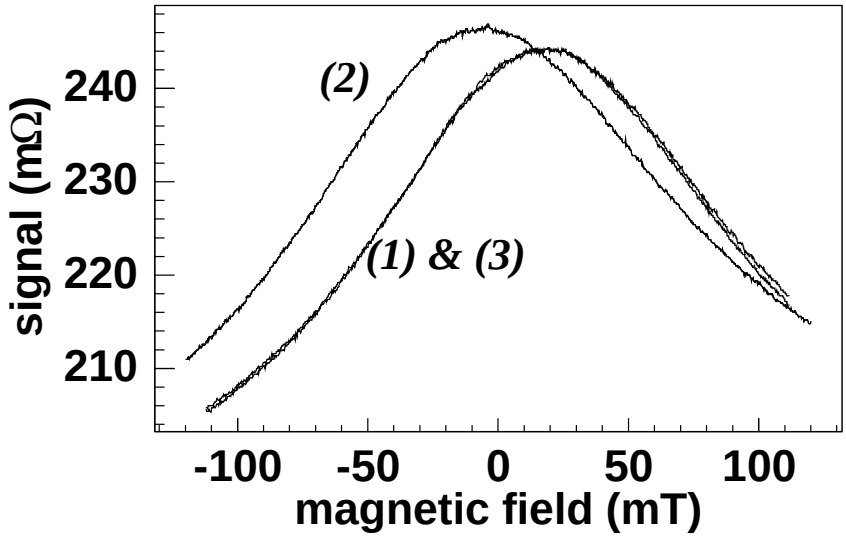

Figure 3.14: Precession measurements in the antiparallel side configuration to show the reciprocity theorem: curve (1) is measured with magnetic field applied in the **z** direction, (2) is measured after interchange of current and voltage probes and with magnetic field applied in the $-\mathbf{z}$ direction, curve (3) after reversal of all magnetisations, interchange of voltage and current probes and magnetic field in the $-\mathbf{z}$ direction.

larisation in Co/AlO_x/Co magnetic tunnel junctions. However, one has to keep in mind that whereas MTJs have resistance of the order of 10^7 Ω μm^2 (LeClair, 2002), in our case, the need of a relatively high current (100 μA through 150×150 nm^2 junctions) requires the fabrication of transparent interfaces (50 $\Omega\mu$m^2). As discussed in Sect. 2.6, the polarisation has a dependence on the barrier's thickness. Moreover, measurements of our barriers with Al in the superconducting state showed the presence of pinholes in the interface between the two metals.

3.7 The reciprocity theorem for the spin accumulation

There is a well known theorem that in the linear regime, a four-terminal measurement is invariant upon exchange of the voltage and contact probes and magnetic field reversal (Büttiker, 1986, 1988). In the case of magnetic contacts, the reciprocity theorem requires that also all the electrodes' magnetisations have to be reversed.

It is evident from eq. (3.11) that we do not get the same signal if we simply reverse the the magnetisation's directions $\mathbf{s} \rightarrow -\mathbf{s}$ and $\mathbf{d} \rightarrow -\mathbf{d}$, or if we interchange voltage and current contacts $\mathbf{s} \leftrightarrow \mathbf{d}$, even at zero applied field $\mathbf{B} = \mathbf{0}$, because of the presence of the fringe field $\boldsymbol{\omega}_{st}$. The only possible way is to in-

terchange voltage and current contacts *and* flip the electrodes' magnetisation. For the precession measurements, one also has to reverse the direction of the external field.

Fig. 3.14 shows such measurements for the side configuration and different magnetic configurations. We proceed as follows: with the external field applied in the positive $\hat{\mathbf{y}}$ direction, we set the contacts in the antiparallel configuration. We then measure the precession signal (curve 1), by applying the magnetic field in the positive $\hat{\mathbf{z}}$ direction. Next, we exchange the current and voltage probes and we repeat the measurement (curve 2), this time applying the external magnetic field in the $-\hat{\mathbf{z}}$ direction. Next, with the lead interchanged, we apply the field in the negative $\hat{\mathbf{y}}$ direction and we set the device to the antiparallel configuration. Finally, we measure the precession again with the external field in the $-\hat{\mathbf{z}}$ direction (curve 3). We notice that curve 2 has not only an offset in the magnetic field and in the signal, but its shape is also different In fact, in the presence of $\boldsymbol{\omega}_{st} \neq \mathbf{0}$, the last term in eq. (3.11) is not invariant upon exchange $\mathbf{s} \leftrightarrow \mathbf{d}$. From these measurements, we also conclude that the contacts' magnetisation fully reverse.

3.8 Comparison with other devices

We report here some measurements on other devices, both at 4.2 K and at room temperature for comparison.

3.8.1 Spin valve measurements at 4.2 K

Spin valve measurements on a different device with tunnel barriers in the 10 kΩ range, were performed at 4.2 K, shown in Fig. 3.15: here the spin signal is about 250 mΩ in both side and diagonal configurations. In the opposite one, the spin induced signal is 30 mΩ. As opposed to the magnetisation reversal at room temperature, which occurs abruptly in most cases, we note that the switching for the widest electrode occurs with discrete changes, resulting in a step-like spin signal. In the diagonal case, the left peak does not reach full height, probably due to incomplete reversal of one of the wide electrodes.

We show now measurements on a H-shaped device at 4.2 K, see Fig. 3.16. The idea is to increase the spin signal by reducing the volume of the island ($R_s \propto \hat{V}^{-1}$). This is the reason to adopt a different layout. Spin valve traces are in Fig. 3.17. However concluding evidence cannot be drawn, because the device was incorrectly positioned away form the middle of the coil, and we could not saturate the ferromagnetic electrodes. The thick trace in left panel shows the first measurement after cool down, with a spin signal as large as 400 mΩ, but subsequent measurements recorded a lower amplitude of the spin signal, 250 mΩ, and a different background. The right panel shows a measurement in the diagonal measuring configuration, with a spin signal comparable to that of the side configuration. Note that the background resistance in both side and diagonal measuring configurations is the result of the changed island geometry. The magnetic field in both panels is estimated taking into account the position of the device outside the coil.

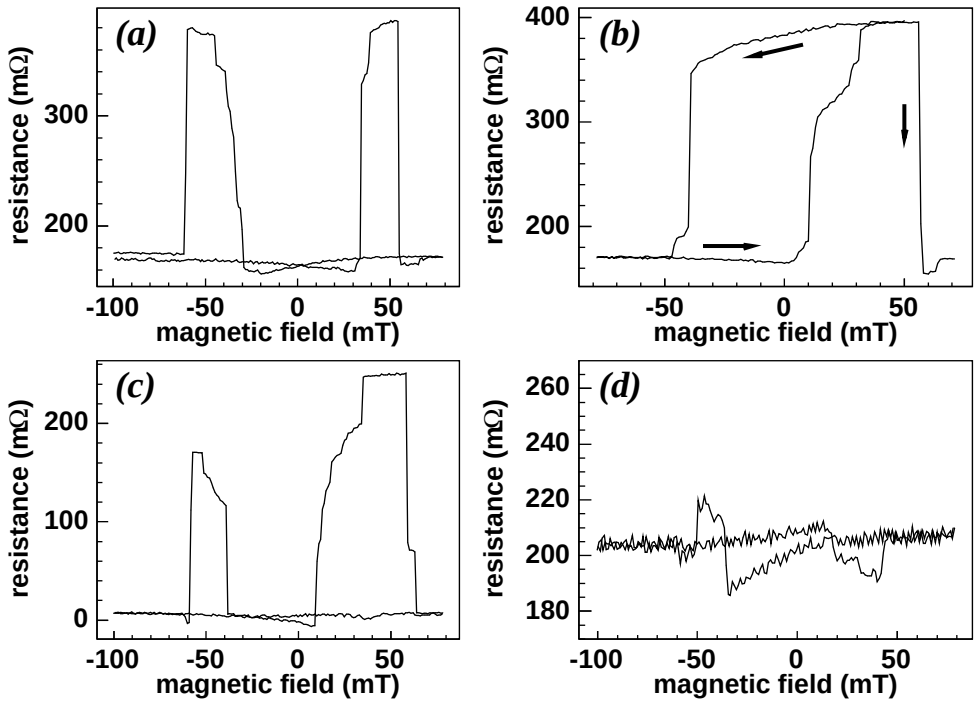

Figure 3.15: Spin valve measurements (a) side, c) diagonal, d)opposite) and memory effect (b) at 4.2 K in a device with tunnel barriers of 20 kΩ.

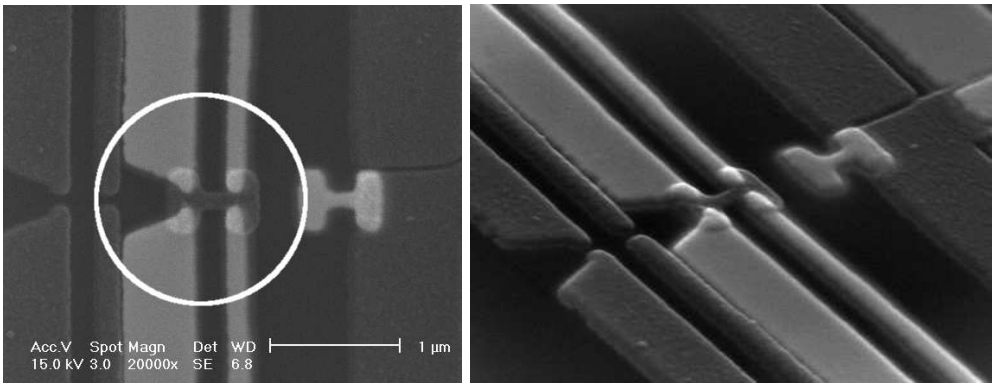

Figure 3.16: SEM micrographs of the H–shaped island device. Encircled in the left panel, is the island. On the right, a different view of the same device.

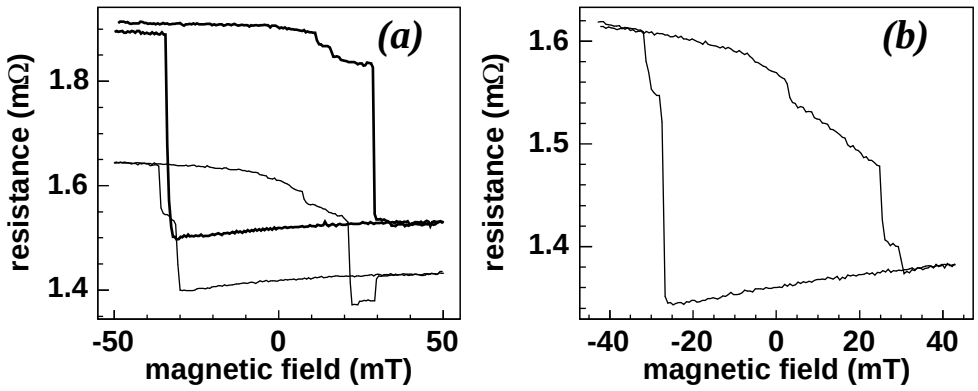

Figure 3.17: Memory effect measurements at 4.2 K on an H-shaped device, in the a) side and b) diagonal measuring configuration. Because of the different layout of the island, Ohmic background is here present in both configurations. The thick trace in the left panel is the first measurement after cool down, with a spin signal of 400 mΩ. Subsequent measurements (thin line in the left and right panels) showed a spin signal of 250 mΩ. The likely reason is the misplacement of the device in the magnetic coil resulting in the magnetic field being not sufficient for complete saturation of the ferromagnetic electrodes. For this reason, we plot the resistance vs the magnetic field scaled by a factor 0.2. The tunnel barrier resistances are in the range 7–12 kΩ.

Spin valve measurements at 4.2 K: comparison with room temperature measurements

Two devices with tunnel barriers have been measured both at 300 K and 4.2 K. Fig. 3.18(a) shows a spin valve measurement in the diagonal configuration at 4.2 K, with a spin signal of ≈ 300 mΩ, that halves at room temperature in both diagonal (bottom trace) and side (top) measuring configuration. The device had tunnel barriers of 15–35 kΩ. The second device (tunnel barrier resistances 5–11 kΩ) showed a ratio of 2.7:1 between the spin signal at 4.2 K, 250 mΩ and at 300 K, 90 mΩ. Only qualitative comparisons can be done here, as the temperature dependence of P and $\tau_{\rm sf}$ separately are not known.

Spin valve measurements at 4.2 K: comparison with the clean contacts devices

As a comparison, we also measured two devices with clean contacts. Fig. 3.19 reports spin valve data for the side (a), opposite (b) and diagonal (c) configurations of one device at 4.2 K and diagonal (d) and opposite (e) at room temperature. Note also that the amplitude of the spin signal is strongly dependent on the measuring configuration. The detected signal above the background is almost two orders of magnitude smaller than in the devices with tunnel barriers. The reason for this is a reduction of the injector and detector polarisations (see Sect. 2.5), as the ferromagnet in direct contact to the non-magnetic metal provides an extra channel for spin relaxation, eq. (2.19).

On the other hand, one has to be careful in interpreting the signal as totally

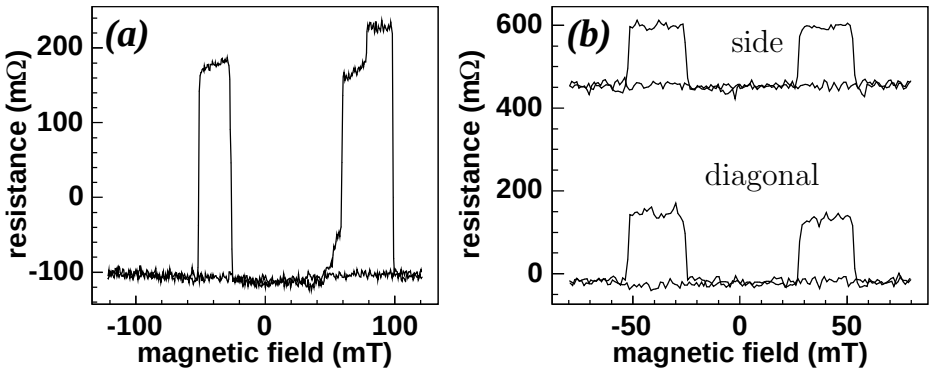

Figure 3.18: Spin valve measurement at 4.2 K in the diagonal configuration (a) and (b) at 300 K in the diagonal and side configuration. The spin signal increases by a factor 2 upon cooling of the device.

induced by spin accumulation. As mentioned above, AMR can give spurious contributions, both at the current and at the voltage contacts: in the first case, it modifies the current path. In the second case, the current partially also flows in the ferromagnetic electrode (even though the *net* current entering the FM voltage contact is null), in a ratio given by the ratio of the conductances of the two metals, Co:Al ≈ 0.2. During magnetisation reversal, the ferromagnet resistance changes due to AMR, about 1% of the Co resistance per square, 5 Ω. For a rough estimate of the spurious contribution δR, we assume that the current path in the island is not affected by the small change in resistance of the ferromagnet; from size considerations, we estimate the fraction of the total current flowing in the contacts region to be 0.1. We obtain $\delta R \approx 0.2 \times (1\% \times 5\ \Omega) \times 0.1$ of the order of 1 mΩ.

Another not understood feature is the absence of any temperature dependence in the spin signal, in Fig. 3.19, whereas the Ohmic background resistance doubles in both (diagonal and opposite) measuring configurations.

3.9 Conclusions

The analysis of spin injection/detection simplifies when using high resistance spin selective interfaces for injection/detection and if the region in which the spin accumulation is created is smaller than $\lambda_{\rm sf}$. In this case, the spin accumulation does not depends on the transport properties, and can be described in terms of two competing processes: the injection of spins, and their dynamics and relaxation mechanisms. The experimental results in this Chapter were interpreted in the light of this observation.

The aluminium island behaves as a zero dimensional system with respect to the spin transport: in fact, measurements in the side and the diagonal measuring configurations report peaks with approximatively the same height, implying that the spin accumulation is uniform within the island. This is consistent with the fact that all lateral dimensions are shorter than $\lambda_{\rm sf} = \sqrt{D\tau_{sf}}$. Here

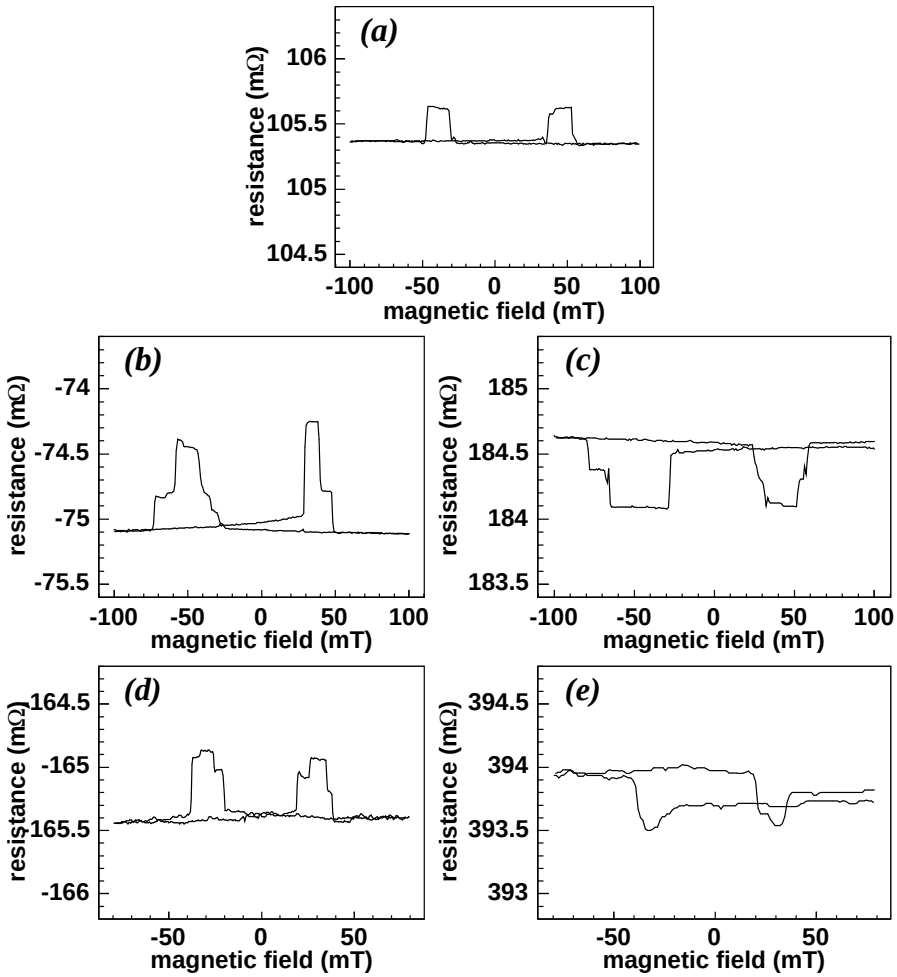

Figure 3.19: Measurement on a clean contact device at 4.2 K in the a) side b) diagonal and c) opposite configurations. d) and e) are measurements taken at 300 K in the diagonal and opposite configurations respectively. Note the absence of any temperature dependence of the spin signal, but a doubling of the four terminal Ohmic resistance.

D was measured on a similar piece of Al and $\tau_{\rm sf}$ as obtained from previous measurements (Jedema *et al.* (2002a) and this thesis). A third direct evidence that the system is 0D comes from $|R_{AP} - R_{anom}| \gg |R_P - R_{anom}|$ that is equivalent to the condition $\tau_{\rm sf} \gg \tau_D$.

Precession measurements with the magnetic field perpendicular to the substrate plane give information on the magnitude of P and $\tau_{\rm sf}$. Furthermore, they allow to determine the relative angle between injectors and detectors. Precession measurements with an in-plane magnetic field could not be performed because of the tendency of the electrodes' domains to change orientation.

Having determined that the electrodes' magnetisations are not collinear to each other, we tested the prediction of the reciprocity theorem, asserting that in the linear regime, the four terminal conductance does not change if voltage and current probes are interchanged, as well as *all* magnetisations are reversed: we found experimentally that it is the case.

Other measurements reported at the end of the Chapter want to be complementary to the previous measurements, as we could not perform an exhaustive set of measurements. In particular, we have shown that the spin signal qualitatively scales with the island's volume, and that the spin induced signal doubles upon cooling of the device.

In the devices with clean contacts, the results were less clear. In contrast to the experiment of Jedema *et al.* (2001), in which the geometry of the system was well defined, and so was the current path, in our case, a detailed analysis requires a numerical solution of the diffusion equation in the island, with the inclusion of the contacts. Moreover, the four terminal signal was probably a combination of spin signal and interface effects (AMR has the same order of magnitude as the peaks height). Even though the peaks at positive and negative fields have equal height they differ significantly for the different measuring configurations, in particular for the side and opposite configurations.